JACS Au
AN OPEN ACCESS JOURNAL OF THE AMERICAN CHEMICAL SOCIETY

pubs.acs.org/jacsau
Article

Engineering Bacterial Biofilm Development and Structure via Regulation of Silver Nanoparticle Density in Graphene Oxide Composite Coating

Shanshan Wang, Shima Liu,* Shuting Cao, Yunhui Bao, Lihua Wang, Zhengliang Eric He, Jiang Li, Yi Zhou,* and Min Lv*

Cite This: JACS Au 2024, 4, 855−864
Read Online
ACCESS | Metrics & More | Article Recommendations | Supporting Information

ABSTRACT: Graphene-based composites have shown significant potential in the treatment of biofilm infections in clinical settings due to their exceptional antimicrobial properties and specific mechanisms. Nevertheless, a comprehensive understanding of the influence exerted by nanoparticles embedded in the composites on the development and structure of biofilms is still lacking. Here, we fabricate different graphene oxide-silver nanoparticle (GAg) composite-modified substrates (GAgS) with varying densities of silver nanoparticles (AgNPs) and investigate their effects on planktonic bacterial adhesion, subsequent biofilm formation, and mature biofilm structure. Our findings indicate that the initial attachment of *Pseudomonas aeruginosa* cells during biofilm formation is determined by the density of AgNPs on the GAgS surface. In contrast, the subsequent transition from adherent bacteria to the biofilm is determined by GAgS's synergistic antimicrobial effect. There exists a threshold for the inhibitory performance of GAgS, where the 20 $\mu g/cm^2$ GAg composite completely prevents biofilm formation; below this concentration, GAgS delays the development of the biofilm and causes structural changes in the mature biofilm with enhanced bacterial growth and increased production of extracellular polymeric substance. More importantly, GAgS have minimal impact on mammalian cell morphology and proliferation while not inducing hemolysis in red blood cells. These results suggest that GAg composites hold promise as a therapeutic approach for addressing medical devices and implant-associated biofilm infections.

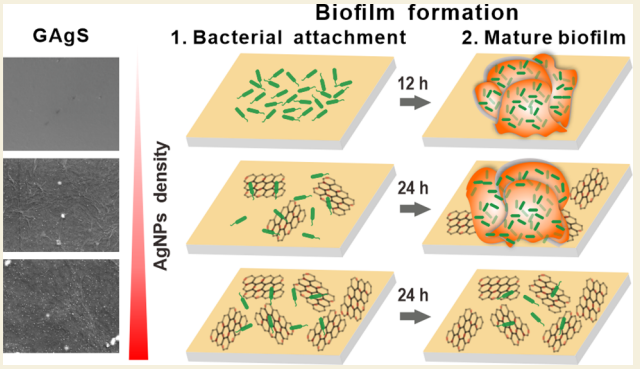

KEYWORDS: *graphene oxide-silver nanoparticle composite, silver nanoparticle density, antimicrobial coating, biofilm*

INTRODUCTION

Bacterial biofilms causing implant-associated infections, such as those related to catheters, pacemakers, and orthopedic implants, pose a significant threat to human life and the healthcare system.[1−3] Planktonic microorganisms that evade the host defense system can attach to the surface of an implant and subsequently proliferate into a dense biofilm within the body. This surface-associated microbial community is embedded in viscous extracellular polymeric substances (EPS) consisting of polysaccharide, protein, and extracellular DNA (eDNA), which provide bacteria with 10−1000 times greater tolerance against detrimental invasions like antibiotics and other bactericides.[4,5] To date, the clinical management of implant infections has predominantly relied on the administration of high-dose antibiotics and implant retention surgery, yielding a success rate of less than 20% in certain cases.[2,6] In most scenarios, the surgical removal of infected implants is necessary. However, compared with eradicating biofilms, preventing their formation represents a more efficient and cost-effective strategy. One approach to hinder the adhesion and colonization of planktonic bacteria onto implants involves incorporating an antimicrobial surface onto the device. Over the past few decades, various antimicrobial agents such as antibiotics,[7,8] peptides,[9,10] polymers,[11−13] and nanoparticles[6,14] have been utilized for modifying implants and creating bactericidal coatings.[15−18] These functionalized implants can effectively impede the initial adhesion of planktonic bacteria while also inactivating surface-adherent bacteria to disrupt biofilm development.

The graphene oxide-silver nanoparticle composite (GAg) has gained significant attention as a highly efficient bactericide

Received: January 3, 2024
Revised: February 3, 2024
Accepted: February 6, 2024
Published: February 16, 2024

https://doi.org/10.1021/jacsau.4c00008
JACS Au 2024, 4, 855−864

Scheme 1. AgNP Density of GAgS Affects Biofilm Formation and Cell Proliferation

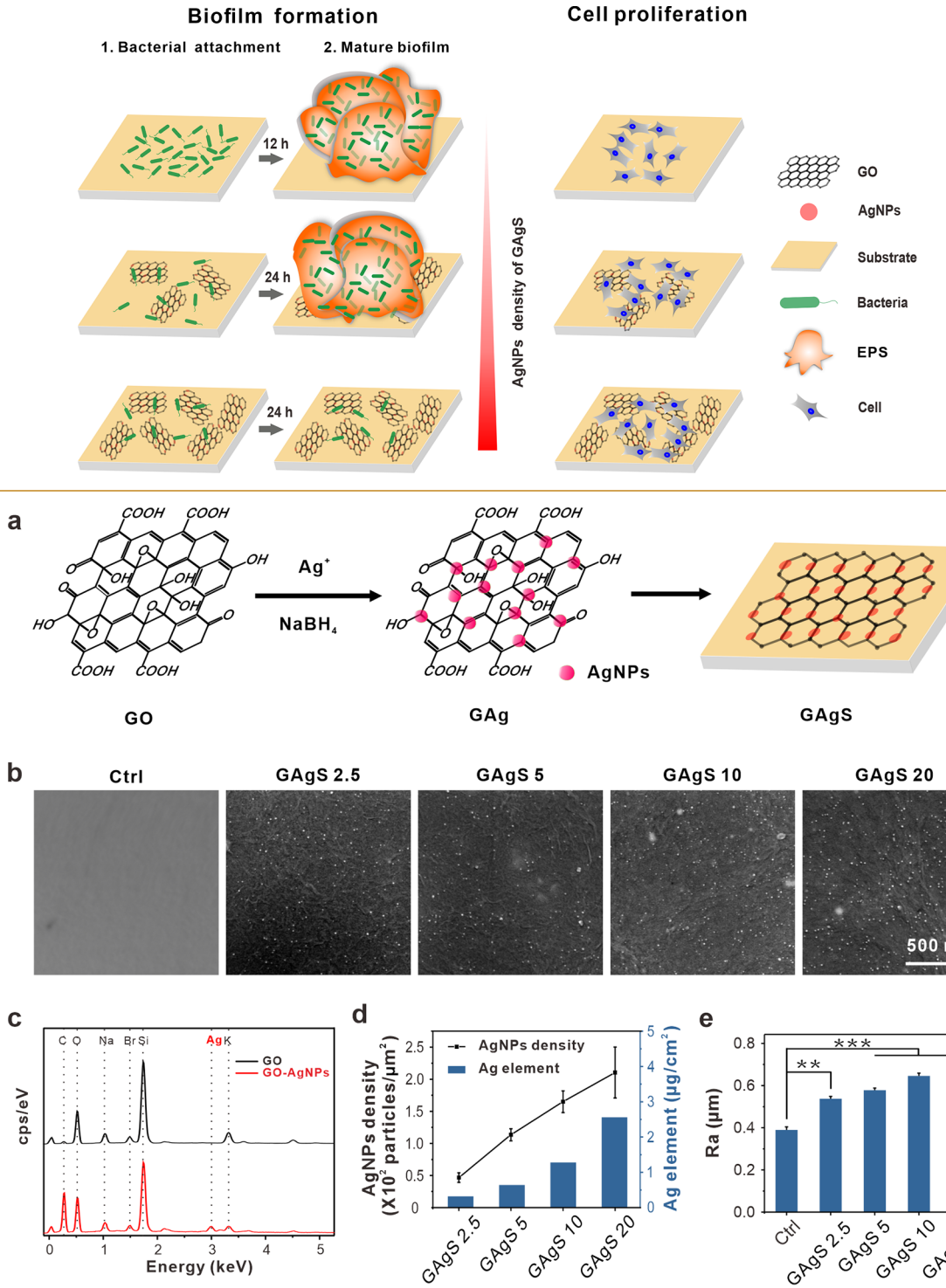

Figure 1. Synthesis and characterization of GAgS.(a) Schematic image of GAg and GAgS preparation. (b) SEM images of GAg substrates. (c) EDS spectra of graphene-based substrates. (d) Density of Ag particles and content of the Ag element on different substrates. (e) Roughness of GAg substrates. Asterisks denote significantly increased roughness as compared with the control group (**$P < 0.01$, ***$P < 0.001$).

in the past decade.[19−22] Its exceptional antibacterial activity can be attributed to its specific physicochemical properties. On one hand, graphene oxide (GO) sheets serve as growth templates that effectively protect silver nanoparticles (AgNPs) from oxidation and aggregation, thereby maintaining their high antibacterial capability.[23] On the other hand, GO sheets possessing a large surface area and abundant functional groups exhibit enhanced affinity toward bacteria, thereby facilitating direct interaction between bacteria and AgNPs, consequently leading to a unique "capture-kill" mechanism against bacterial pathogens. Moreover, GO itself exhibits remarkable bactericidal properties through oxidative stress and physical damage. To date, the GAg composite has demonstrated efficacy in effectively inactivating various planktonic microorganisms,

https://doi.org/10.1021/jacsau.4c00008
JACS Au 2024, 4, 855−864

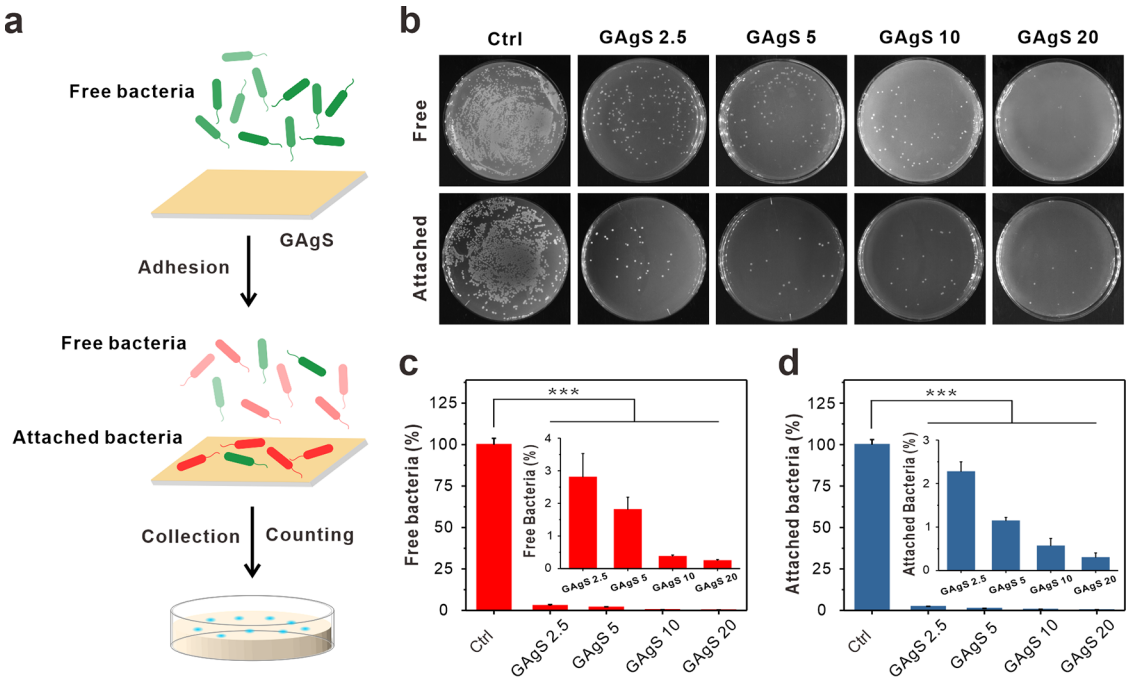

Figure 2. Adhesion capability of planktonic *P. aeruginosa* on GAgS. (a) Schematic of bacterial adhesion at the initial stage of biofilm formation. (b) Growth of free and attached *P. aeruginosa* on GAgS after 2 h. The number of (c) free and (d) attached bacteria on GAgS. Insets provide an enlarged depiction of the bacteria rate of GAgS. Asterisks denote significantly reduced bacteria as compared with the control group (***$P < 0.001$).

including pathogenic bacteria, fungi,[24] and even viruses.[25−27] Furthermore, it exhibits inhibitory effects on biofilm formation and possesses a remarkable capacity for eradicating biofilms. It has been reported that GAg dispersion can eliminate 100% of *Pseudomonas aeruginosa* (*P. aeruginosa*) cells adhered to a stainless steel surface within 1 h.[28] The complex also exhibits remarkable efficacy in eliminating adherent cells from both Gram-positive and Gram-negative microbial strains.[29] Importantly, GAg has been successfully integrated into the polymer film or applied as coatings on various substrates to effectively inhibit biofilm formation in diverse fields such as biomedicine,[30,31] marine antifouling,[32−34] and wastewater treatment.[35] Undoubtably, GAg is an ideal antimicrobial coating with robust antibiofilm activity. However, previous studies have exclusively focused on the antibiofilm efficacy and potential application of this composite, offering limited information on the effects of the GAg-modified substrate (GAgS) on planktonic adhesion and subsequent biofilm development. This knowledge gap, particularly in relation to the potential influence of different components on antibiofilm efficacy, such as the density of AgNPs in the composites, requires further investigation.

In this study, GAg coatings with different densities of AgNPs were prepared by deposition followed by vacuum drying, and their effects on biofilm formation and cell proliferation were investigated (Scheme 1). The adhesion of planktonic bacteria is effectively inhibited by GAgS, mainly due to the density of AgNPs rather than the toxic effect of GAg. However, GAg synergistically affects the ability of adherent bacteria to form the biofilm and the architecture of the mature biofilm. A concentration of 20 $\mu g/cm^2$ GAg on the substrate surface completely inhibits biofilm formation; below this concentration, GAg coatings only delay biofilm formation but promote bacterial proliferation and EPS production in the mature biofilm. In contrast, GAgS show no toxicity to the proliferation of preosteoblast cells. These findings provide valuable insights into developing advanced strategies against biofilm-associated infections.

RESULTS AND DISCUSSION

Synthesis and Characterization of the GAg Substrate

GAg composite-modified substrates were fabricated according to the procedure shown in Figure 1a. The GAg composite was synthesized through the reduction of silver ions on the surface of graphene oxide as previously reported.[36] The synthesized GAg solution was deposited onto a glass substrate and dried under vacuum conditions. By adjusting the concentration of GAg on the surface, we obtained GAgS with varying densities of Ag nanoparticles, namely, GAgS 2.5, GAgS 5, GAgS 10, and GAgS 20 for concentrations of 2.5, 5, 10, and 20 $\mu g/cm^2$, respectively. Scanning electron microscopy (SEM) images revealed that the four GAgS exhibited wrinkles with white spots compared to the smooth glass control, and the density of shite spots increased with the GAg concentration (Figure 1b). Energy-dispersive spectrometry (EDS) analysis confirmed the successful formation of GAgS by detecting a characteristic peak at an energy of 3 keV corresponding to the Ag element (Figure 1c).[32,34] The presence of randomly dispersed white dots on the background indicated stable anchoring AgNPs on the GO surface during interface modification. The densities of AgNPs were determined to be approximately 47, 113, 165, and 210 particles/μm^2 for GAgS 2.5, GAgS 5, GAgS 10, and GAgS 20, respectively. The amount of Ag element in GAgS 20 was as low as 2.56 $\mu g/cm^2$ (Figure 1d). We subsequently measured the interfacial hydrophobicity and roughness as they play significant roles in biofilm formation at the initial stage including bacterial adhesion and growth.[37,38] GAg modification has minimal impact on substrate hydrophilicity (Figure S1), but it did increase surface roughness (Figure S2 and Figure 1e). Higher concentrations of GAg resulted in greater

https://doi.org/10.1021/jacsau.4c00008
JACS Au 2024, 4, 855−864

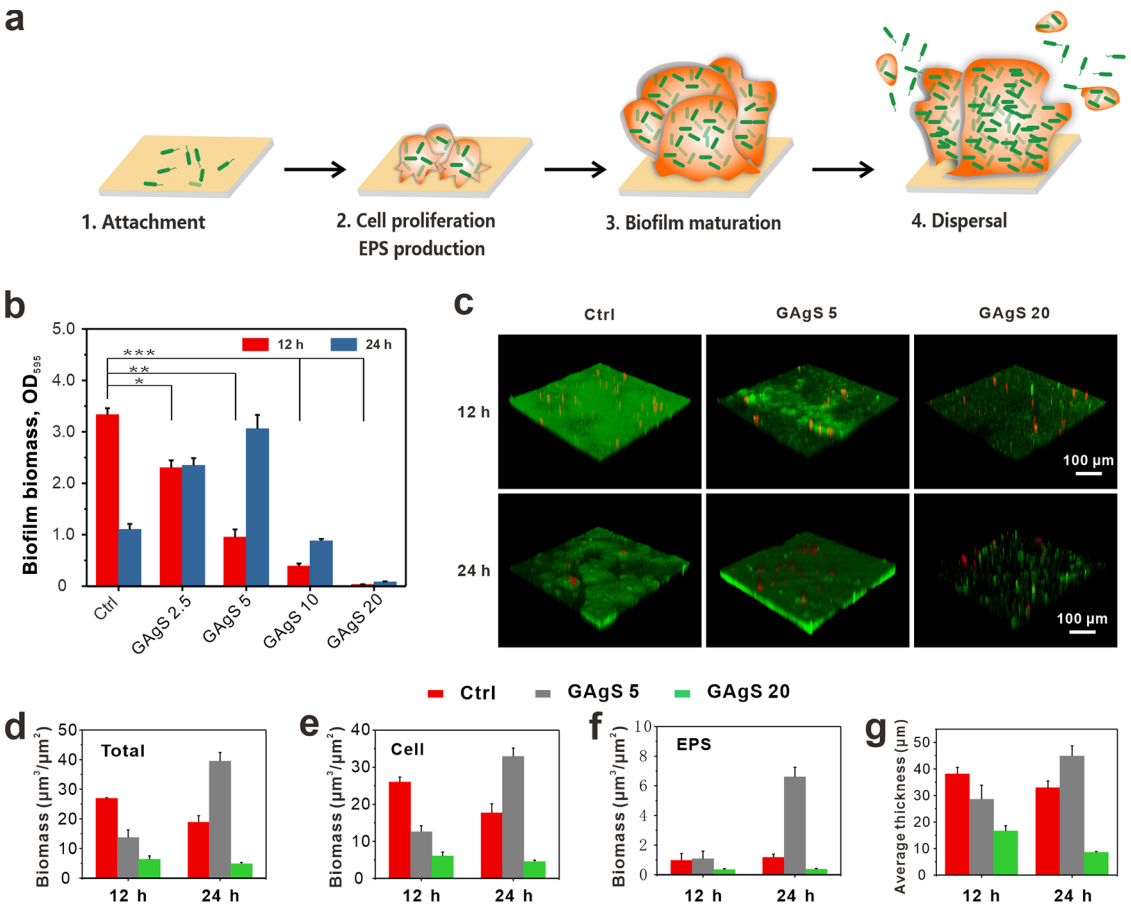

Figure 3. Development of the biofilm on GAgS. (a) Schematic of biofilm development. (b) Effects of different concentrations of the GAg substrate on biofilm formation. (c) 3D confocal images of the biofilm. (d) Total biomass, (e) cell biomass, (f) EPS biomass, and (g) thickness of the biofilm at different culture times. Asterisks denote significantly inhibited biofilm biomass as compared with the control group (*$P < 0.05$, **$P < 0.01$, ***$P < 0.001$).

roughness, which can be attributed to the wrinkled GO of GAg (Figure S3). Collectively, these results indicate the successful preparation of GAgS with different surface properties.

Adhesion of Planktonic Bacteria on GAgS

The irreversible adhesion of planktonic bacteria to a biotic or abiotic interface is a critical step in biofilm formation. To investigate the effect of GAgS on bacterial adhesion, we incubated Gram-negative *P. aeruginosa* with GAg-coated and uncoated substrates for 2 h and then counted the number of unattached (free) and attached bacteria cells using the plate-counting method (Figure 2a). The results demonstrated a pronounced inhibitory effect of all GAg substrates on both free-floating bacteria and bacteria adhered to the substrates (Figure 2b). As the dosage of GAg increased, a gradual reduction in the number of free (Figure 2c) and attached (Figure 2d) cells was observed compared to the control group. Adhesive bacteria on GAgS 2.5, GAgS 5, GAgS 10, and GAgS 20 were reduced by 97.97 ± 0.23, 98.86 ± 0.08, 99.44 ± 0.17, and 99.70 ± 0.11%, respectively; no statistically significant difference was found among them. This suggests that GAgS can significantly inhibit the initial adhesion of planktonic bacteria.

Biofilm Formation and Architecture on GAgS

Next, to assess the capacity of attached bacteria on various substrates to mature into the biofilm after cellular proliferation and EPS secretion (Figure 3a), we quantified the biomass of the biofilm using crystal violet staining after 12 and 24 h. As depicted in Figure 3b, bacteria cultivated on glass coverslips as the control group had successfully developed into a mature biofilm within 12 h, which is consistent with our previous findings.[36] However, there was a noticeable delay in the biofilm development for bacteria adhered to different GAg substrates. This delayed effect became more pronounced with an increasing GAg dosage. After culturing for 24 h, the control biofilm entered the dispersal phase with a significant reduction in biomass. Bacteria cultured on GAgS 5 approached maturity similar to that observed at 12 h for the control biofilm. With the exception of bacterial growth being completely inhibited on GAgS 20, adhesive bacteria on all other GAgS exhibited slow development within 24 h.

To observe the architecture of the biofilm grown on GAgS, we used fluorescent SYTO9 (green) and Concanavalin-A Alexa Fluor (red) probes to label live bacteria and EPS, respectively.[36] SYTO 9 has the ability to penetrate the cell membranes of live bacteria and bind to their DNA molecules. Concanavalin-A is commonly used as an EPS probe due to its selective binding affinity toward polysaccharides. Figure 3c illustrates that compared to the control biofilm, the biofilm on the GAg substrate exhibited a lower bacterial count and a less compact structure after 12 h. After 24 h, bacterial cells started dispersing from the control biofilm; in contrast, GAgS 5 displayed a dense and mature biofilm structure similar to the control at 12 h. Only a few bacteria were observed on GAgS 20

https://doi.org/10.1021/jacsau.4c00008
JACS Au 2024, 4, 855−864

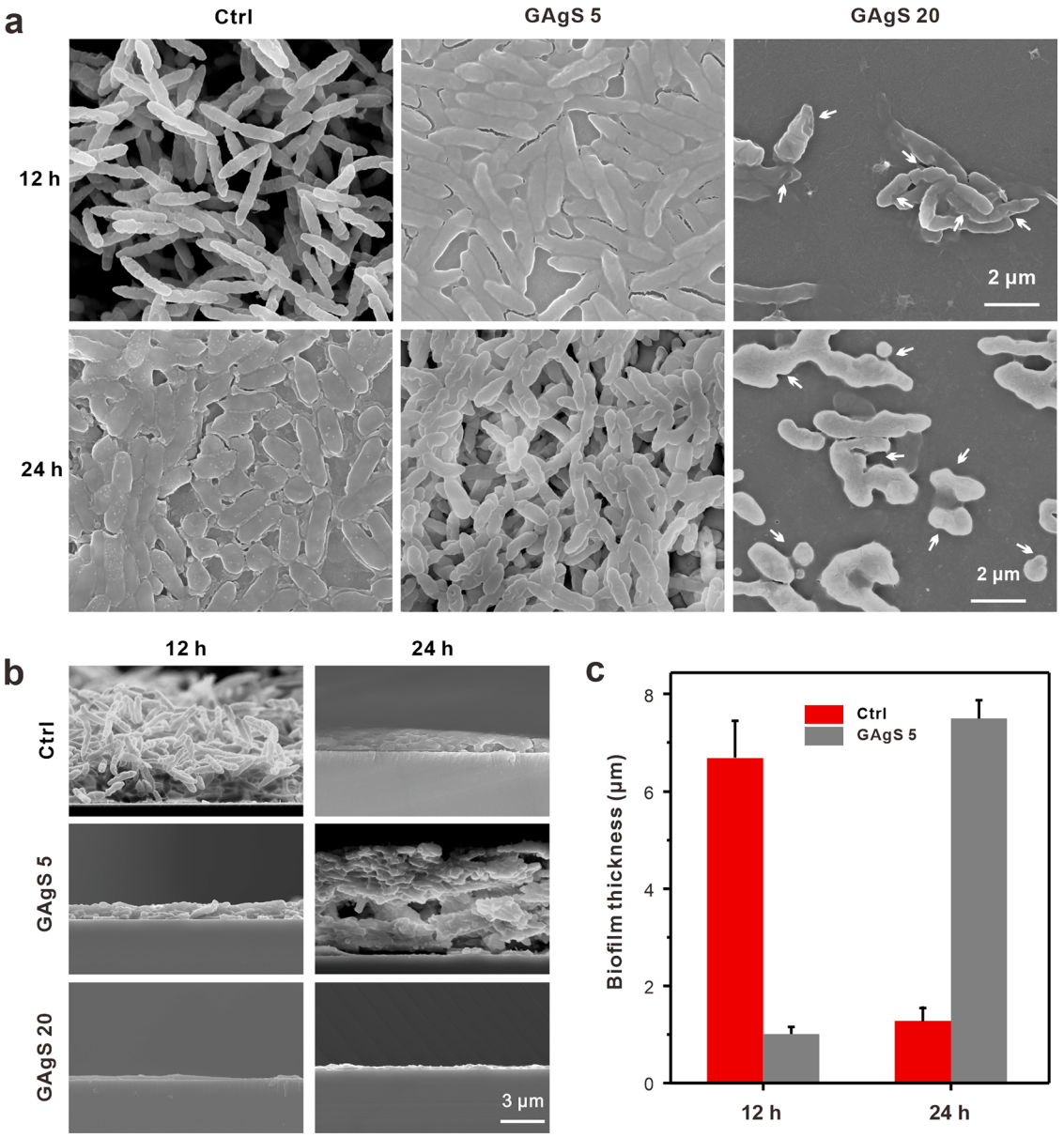

Figure 4. Structure of the biofilm observed by SEM. (a) Top and (b) lateral images of the biofilm on different substrates for 12 and 24 h. (c) Quantification of biofilm thickness in lateral SEM images.

for the entire 24 h period, indicating significant inhibition in biofilm development. Quantitative data showed that GAgS 5 had a higher total biomass than the control at the mature stage (Figure 3d), not only in bacteria biomass (Figure 3e) but also in the EPS biomass (Figure 3f), indicating its beneficial effect on biofilm formation. Apart from the components of the biofilm, GAgS 5 increased the thickness of the biofilm in the mature stage (Figure 3g), suggesting that GAgS 5 also affected the spatial structure of the biofilm. However, the biofilm formation on the GAgS 20 was significantly inhibited due to the high toxicity of GAgS 20 to bacteria (Figure 3d–g).

SEM images further confirmed the results from the confocal analysis. As depicted in Figure 4a, the *P. aeruginosa* biofilm formed on both a glass substrate and GAgS 5 exhibited a typical multilayered structure, with rod-shaped bacteria observed after 12 and 24 h cultures. In contrast, the adherent bacteria in the GAgS 20 group displayed fracturing and deformation (indicated by white arrows) with minimal proliferation. Lateral images revealed that the thickness of the control group was significantly higher than that of the GAgS 5 group at 12 h (Figure 4b), measuring at 6.68 ± 1.52 and 1.01 ± 0.14 μm, respectively (Figure 4c). Conversely, the thickness of biofilms formed under these two conditions was reserved at 24 h; a reduced thickness of the normal biofilm was observed as it entered the dispersal stage. The mature biofilm supported by GAgS 5 showed an increased thickness compared to the control group after 12 h. Bacteria in the GAgS 20 group were unable to form a three-dimensional (3D) biofilm structure within 24 h. This finding is consistent with the quantitative analysis of confocal images (Figure 3g).

Biocompatibility of GAgS

To evaluate the potential application of GAg as an antimicrobial coating in biomedicine, the toxic effects of GAgS on osteoblast precursor MC3T3-E1 cells were examined by an MTT assay and live/dead cell staining. The viabilities of cells grown on GAgS 2.5, GAgS 5, GAgS 10, and GAgS 20

https://doi.org/10.1021/jacsau.4c00008
JACS Au 2024, 4, 855–864

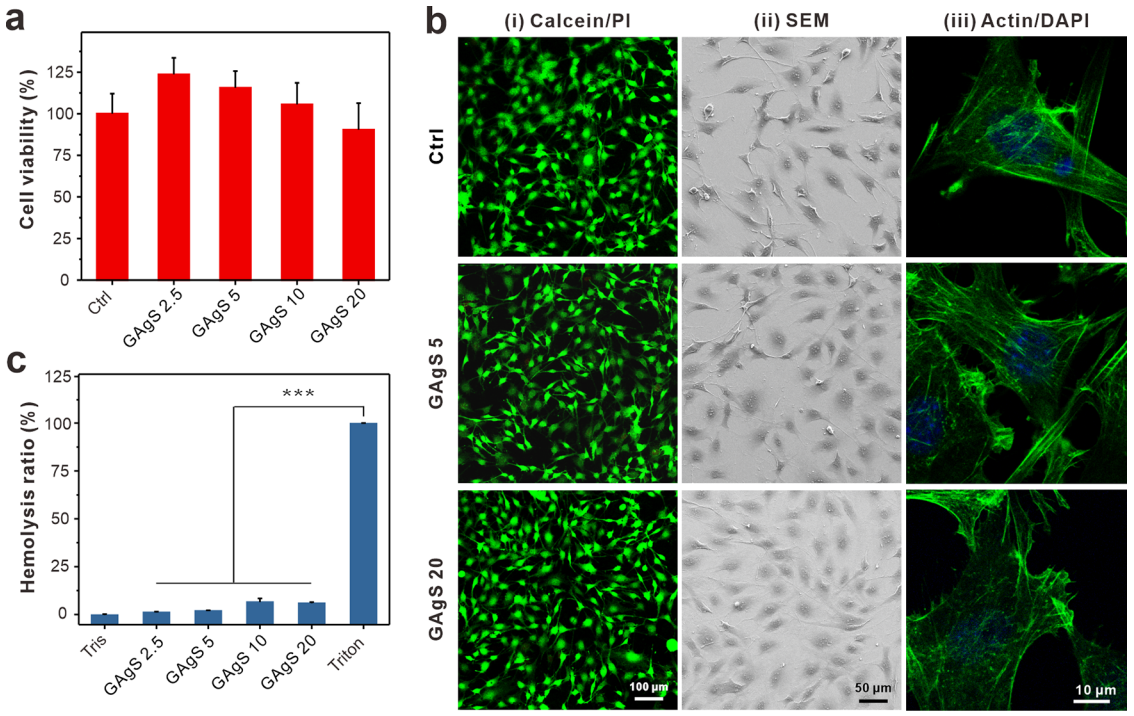

Figure 5. Biocompatibility of GAgS. (a) Cell viability of MC3T3-E1 cells grown on different substrates. (b) Cellular morphology on the substrate with and without GAgS. (i) Calcein/PI staining. (ii) SEM imaging. (iii) Actin immunofluorescence staining (green) and nuclei (blue). (c) Hemolytic toxicity of different GAgS. Triton as the positive group; Tris buffer as the negative group. Asterisks represent significantly reduced hemolysis as compared with positive control (***$P < 0.001$).

were 123.6, 115.7, 105.6, and 90.4% compared to the coverslip (Figure 5a), respectively. Except for high toxic GAgS 20, the number of cells grown on other GAgS was higher than that in the control group due to a slight roughness of GAgS, which was more conducive to cell adhesion and growth.[39,40] To further evaluate cellular viability, the Calcein-AM probe was utilized for labeling live cells due to its facile internalization into the cell and subsequent hydrolyzation by intracellular esterase, resulting in strong green fluorescence emission. However, the red fluorescent PI can only penetrate damaged cell membranes to bind to nucleic DNA, serving as a probe for dead cells. No discernible red fluorescence was observed in any GAgS groups (Figure 5b(i) and Figure S4), indicating that GAgS does not exhibit cytotoxicity. The morphology of the MC3T3-E1 cells was examined using SEM and immunofluorescence staining. There were minimal differences in cellular morphology among all groups (Figure 5b(ii)). ActinGreen with green fluorescence labels cellular actin (microfilaments), while blue DAPI labels intracellular DNA within the nucleus. As shown in Figure 5b(iii), compared with the control group, there were no significant differences in microfilaments or synapses of cells grown on GAgS. This suggests that GAg substrates have a negligible effect on preosteoblast growth.

In addition, a hemolysis assay was conducted to further examine the biocompatibility of GAgS. As depicted in Figure 5c, compared to the approximately 100% hemolysis rate of Triton (positive control), the hemolysis rate of GAgS did not exceed 10% after 1.5 h of incubation with blood cells. These findings strongly suggest that the GAg substrates exhibit excellent biocompatibility and hold great potential as a coating material for medical devices.

Biofilm infections on medical implants and devices have seriously threatened public health globally.[1,2] Instead of relying on antibiotics and surgery to eliminate the formed biofilm, it is crucial to develop a bactericidal coating to prevent planktonic bacteria from developing into a biofilm.[15,16] There is no doubt that the GAg composite is one most famous biocides to fabricate antimicrobial coating to prevent biofilm infection.[32,34] Previous studies mostly focused on whether GAg inhibits biofilm formation or eradicates formed biofilms. GAg with more stable and superior biocidal activities has been reported and used to fight against various microorganism biofilms.[28,29] In fact, it is equally important to investigate how GAg affects the process of biofilm formation, which involves adhesion of planktonic bacteria, bacterial proliferation and EPS production, biofilm maturation, and dispersal for initiating new generation.[1,2] In this study, we employed a facile deposition method to fabricate GAg and successfully generated diverse antimicrobial coatings with varying densities of AgNPs and interfacial roughness. The results indicated that GAgS had an excellent ability to hinder the attachment of planktonic bacteria. The surface roughness of the substrate plays a crucial role in bacterial adhesion,[38,41] but it does not lead to bacterial inactivation. GAgS 2.5, containing 2.5 $\mu g/cm^2$ for GAg, demonstrated unprecedented antibacterial efficacy by effectively inactivating over 97% of free and attached bacteria within 2 h. However, the enhanced inhibitory efficacy of GAg against bacterial adhesion with increasing concentrations of GAg modification at the interface was not observed here. The findings of our study suggest that the interfacial roughness and GAg concentration are unlikely to be significant factors in inhibiting bacterial adhesion. We hypothesized that the high density of Ag particles per unit area was responsible for the remarkable inhibitory efficacy of GAgS 2.5. SEM images

https://doi.org/10.1021/jacsau.4c00008
JACS Au 2024, 4, 855−864

showed approximately 47 particles/μm^2 on the surface of GAgS 2.5 (Figure 1b,d). When a bacterium attached to GAgS 2.5 in parallel, it was estimated to come into contact with approximately 50 Ag nanoparticles under our experimental conditions. The strong direct interaction between immobilized AgNPs and bacteria can compromise bacterial integrity,[29,36] leading to the presence of numerous dead bacteria in the culture medium (Figure 2c). As a result, only a limited number of bacteria can survive and settle in GAgS (Figure 2d).

Attached bacteria proliferate and produce EPS, ultimately forming a 3D biofilm. Bacterial daughter cells expand laterally and vertically, which is influenced by ambient conditions like interfacial properties and bactericides.[5] Surviving adhesion bacteria on GAgS interact not only with Ag nanoparticles but also with GO sheets during biofilm formation. The entire process is influenced by all components within the GAg composite, rather than any individual component. In addition, there exists a critical threshold of GAgS (20 $\mu g/cm^2$) that determined the transition from adherent bacteria to mature biofilm. Below this threshold, bacteria have the ability to adapt to the harsh environment (antimicrobial GAgS) by activating stress response mechanisms such as temporary dormancy and excessive production of EPS.[1,36] This is the reason why bacteria can still form a biofilm on GAgS 5, albeit with delayed growth and increased EPS (Figure 3e–f). In contrast, GAgS 20 effectively inhibits biofilm development, potentially attributed to the physical and oxidative damage mechanisms of GAg.[19,20] Both graphene and AgNPs induce the generation of reactive oxygen species, resulting in bacterial inactivation or metabolic dysfunction that inhibits bacterial division.[42,43] Moreover, it cannot be ruled out that a bactericidal effect occurs due to the release of silver ions from AgNPs. Although these toxic factors also induce apoptosis and death in mammalian cells, their larger size and complex physiology compared to microorganisms enable them to tolerate effective concentrations of antimicrobial agents.[44,45] Therefore, the favorable biocompatibility of GAgS has further confirmed previous reports.[46]

CONCLUSIONS

In summary, we prepared GAg-modified substrates with various densities of AgNPs and systematically investigated their effect on biofilm development. Our results indicate that the high density of AgNPs in GAgS is the key factor in inhibiting the initial attachment of planktonic bacteria compared to other factors, such as the GAgS concentration and interfacial roughness. Subsequent biofilm development from adhesive bacteria on GAgS is determined by the GAgS dosage. The 20 $\mu g/cm^2$ GAg substrate can completely inhibit biofilm formation. Below this concentration, compared to the control group, GAgS only induce the delayed biofilm formation and trigger more EPS production in mature biofilms. Notably, GAgS exhibits no cytotoxicity and hemolysis effect even at the highest concentration of GAg used in this study. These findings demonstrate that GAg substrates have good antibiofilm effects and biocompatibility, indicating significant potential for application as antimicrobial coatings to prevent biofilm-associated infection.

EXPERIMENTAL SECTION

Preparation and Characterization of GAgS

GAg composites were prepared and characterized in our previous study.[36] To fabricate the GAg substrate, 200 μL of GAg solution was dropped onto the surface of a circular coverslip with a diameter of 12 mm uniformly and subsequently dried under vacuum at 60 °C for 12 h. By adjustment of the concentration of GAg, various densities of AgNPs on GAg substrates were achieved.

Surface morphologies were examined using scanning electron microscopy (SEM, LEO 1530vp, Germany) equipped with energy-dispersive spectroscopy (EDS, Oxford) for elemental composition analysis. Four replicate samples were prepared, and more than eight distinct regions were selected from each sample's SEM images to determine the Ag density of GAgS. The contact angle of GAgS was measured using a contact angle measurement (Attension Theta). The surface roughness of GAgS was determined by using a 3D measuring laser microscope (Olympus Lext OLS4100). The amount of Ag element ($C_{Ag/GAg}$) in the GAg solution was determined using inductively coupled plasma mass spectrometry (ICP-MS; Thermo Elemental X Series). The concentration of the Ag element contained in GAgS ($C_{Ag/GAgS}$) was calculated using the following formula:

$$C_{Ag/GAgS} = \frac{VC_{Ag/GAg}}{S}$$

where $C_{Ag/GAg}$ represents the concentration of Ag in the GAg solution modified at the interface; V is the volume of GAg solution used for modification; S corresponds to the surface area covered by GAg on the interface.

Bacteria Culture

Gram-negative *P. aeruginosa* was employed as a model microorganism for biofilm formation. Fresh bacteria were grown on an LB plate and stored at 4 °C. Prior to biofilm growth, a single colony of *P. aeruginosa* was selected and cultivated in an LB medium at a shaker (220 rpm, 37 °C). After overnight incubation, *P. aeruginosa* cells in the logarithmic growth phase were harvested by centrifugation at 10,000 rpm for 1 min and suspended in PBS for subsequent biofilm experiments.

Adhesion of Planktonic Bacteria on GAgS

The sterile coverslip, with or without GAg, was placed in a 24-well plate. Bacteria cells of 1×10^6 CFU/mL in the LBNS medium (3%) were added to each well and cultured at 37 °C for 2 h. Subsequently, the culture medium was collected, and the substrate was gently washed three times with PBS to remove reversibly adherent bacteria. PBS washes were also collected and combined with the culture medium. Finally, adherent bacteria were scraped off from the substrates and collected. The quantity of both unattached (free) and attached bacteria was determined using a plate-counting method.

Biofilm Formation

After 2 h of culture, unattached bacteria were removed, and attached bacteria on the substrate were cultured with the LBNS medium (100%) to form the biofilm. Following incubation of either 12 or 24 h, the development of the biofilm on GAgS was assessed by crystal violet staining, confocal imaging, and SEM imaging.

Crystal Violet Staining

The biofilm adhered to the GAgS was gently rinsed three times with PBS and air-dried for 3 min. Then, the biofilm was stained with 300 μL of 0.1% (w/v) CV at room temperature for 15 min followed by gentle washing with PBS three times. The biomass of the biofilm was quantified using a microtiter plate reader at OD_{595} after dissolving the CV-stained biofilm in 95% ethanol. All measurements were performed in triplicate.

Confocal Imaging

Cultured biofilms were gently rinsed three times with PBS and subsequently stained with SYTO9 (6 $\mu g/mL$, green fluorescence) for 15 min in the dark at room temperature to label live bacterial cells. After gentle washing to remove residual SYTO9, the samples were further stained with a solution of the concanavalin-A–Alexa Fluor 647 conjugate (50 $\mu g/mL$, red fluorescence, labeled EPS) for 15 min. Bacteria and EPS production were visualized by confocal laser scanning microscopy (CLSM, Leica TCS SP8, Germany). The excitation/emission wavelengths of SYTO9 and Alexa Fluor 647 were

https://doi.org/10.1021/jacsau.4c00008
JACS Au 2024, 4, 855–864

480/500 and 650/668 nm, respectively. Stack images of the biofilm were acquired by scanning along the Z axis at intervals of 1.8 μm followed by analysis using COMSTAT software.[36]

SEM Imaging

Biofilms on the GAgS were gently washed three times with PBS followed by fixing with 2% glutaraldehyde at 4 °C for 2 h. Subsequently, the fixed samples were dehydrated through freeze-drying for 24 h. Finally, the samples were coated with gold and observed by using SEM (LEO 1530vp, Germany).

Cellular Growth on GAgS

MC3T3-E1 cells were cultured in minimum essential medium α (MEMα) supplemented with 10% FBS, 1% streptomycin/penicillin, and 1% nonessential amino acid in 5% CO_2 at 37 °C. Sterile coverslips with and without GAg were placed in 24-well plates. MC3T3-E1 cells were seeded into the wells at a density of 5×10^4 cells/well and incubated for 24 h. Cell viability was assessed using the MTT assay. Cell morphology was observed through CLSM and SEM. After the initial culture of 24 h, on one hand, the cells were stained with Calcein-AM (2 μg/mL) and PI (3 μg/mL) for 15 min before being observed using CLSM. The excitation/emission wavelengths of Calcein-AM and PI were 495/515 and 490/635 nm, respectively. On the other hand, the cells were fixed with 2.5% glutaraldehyde overnight at 4 °C and subjected to gradient dehydration with ethanol. All samples were sprayed with gold and observed by SEM (LEO 1530vp, Germany). Additionally, immunofluorescence staining facilitated the visualization of the cellular microfilaments and cell nuclei. The cells were initially fixed with 4% glutaraldehyde followed by ActinGreen staining for microfilaments (300 μL, 2 drops/mL) and DAPI staining for nuclei (300 μL, 1 μg/mL). Subsequently, the samples were observed using CLSM. The excitation and emission wavelengths used for ActinGreen and DAPI were 496/516 and 406/460 nm, respectively.

Hemolytic Toxicity of GAgS

The hemolysis assay was conducted using sheep blood, which was diluted with PBS (1:20) and centrifuged at 1000*g* for 8 min to remove the serum. The collected red blood cells (RBCs) were washed three times with PBS before being added to various concentrations of GAg solution in a 24-well plate. Triton-100 and Tris buffer served as the positive (+) and negative (−) control, respectively. The plate was gently shaken and incubated at 37 °C for 1.5 h. After centrifugation, RBCs were collected, and the absorbance of the supernatant was measured at 570 nm by using a UV−vis spectrometer (Hitachi, U-3010, Japan). The percentage of hemolysis was calculated according to the following formula:

$$\text{hemolysis}(\%) = \frac{A_s - A_{(-)}}{A_{(+)} - A_{(-)}} \times 100$$

where A_s, $A_{(-)}$, and $A_{(+)}$ are the absorbances of GAgS, Tris buffer, and Triton-100, respectively.

Statistical Analysis

Data were presented as mean ± standard deviation. A comparison was made between the values of the experimental groups and control groups. Statistical significance was analyzed by Student's *t* test to identify any statistically significant differences ($p < 0.05$). All experiments were repeated at least three times.

ASSOCIATED CONTENT

Supporting Information

The Supporting Information is available free of charge at https://pubs.acs.org/doi/10.1021/jacsau.4c00008.

Materials used in this work; contact angle of GAgS; 3D measuring laser images of GAgS; SEM image of the GO-coated substrate (PDF)

AUTHOR INFORMATION

Corresponding Authors

Shima Liu − *Key Laboratory of Hunan Forest Products and Chemical Industry Engineering, National and Local United Engineering Laboratory of Integrative Utilization of Eucommia ulmoides, College of Chemistry and Chemical Engineering, Jishou University, Jiajie Zhang, Hunan 427000, China*; Email: liushima@jsu.edu.cn

Yi Zhou − *College of Basic Medicine, Chengdu University of Traditional Chinese Medicine, Chengdu 611137, China*; Email: zhouyi0465@sina.com

Min Lv − *College of Chemistry and Materials Science, Shanghai Normal University, Shanghai 200234, China*; orcid.org/0000-0003-0587-8528; Email: lvmin@shnu.edu.cn

Authors

Shanshan Wang − *College of Chemistry and Materials Science, Shanghai Normal University, Shanghai 200234, China*

Shuting Cao − *Xiangfu Laboratory, Jiashan 314102, China*

Yunhui Bao − *Key Laboratory of Hunan Forest Products and Chemical Industry Engineering, National and Local United Engineering Laboratory of Integrative Utilization of Eucommia ulmoides, College of Chemistry and Chemical Engineering, Jishou University, Jiajie Zhang, Hunan 427000, China*

Lihua Wang − *Institute of Materiobiology, College of Science, Shanghai University, Shanghai 200444, China*

Zhengliang Eric He − *Shanghai Soong Ching Ling School, Shanghai 201703, China*

Jiang Li − *Institute of Materiobiology, College of Science, Shanghai University, Shanghai 200444, China*

Complete contact information is available at: https://pubs.acs.org/10.1021/jacsau.4c00008

Author Contributions

S.L. and M.L. conceived the project and wrote the manuscript. S.W., S.L., and S.C. performed the experiments and analyzed the data. L.W., Z.E.H., Y.B., J.L., and Y.Z. analyzed the data and participated in the discussions.

Notes

The authors declare no competing financial interest.

ACKNOWLEDGMENTS

This work was financially supported by the National Key R&D Program of China (2020YFA0908900), the National Natural Science Foundation of China (32371439, 31971310, and 22274013), and the Research Foundation of Hunan Provincial Education Department (no. 22B0543).

REFERENCES

(1) Arciola, C. R.; Campoccia, D.; Montanaro, L. Implant Infections: Adhesion, Biofilm Formation and Immune Evasion. *Nat. Rev. Microbiol.* **2018**, *16* (7), 397−409.

(2) Daubert, D. M.; Weinstein, B. F. Biofilm as a Risk Factor in Implant Treatment. *Periodontology 2000* **2019**, *81* (1), 29−40.

(3) Caldara, M.; Belgiovine, C.; Secchi, E.; Rusconi, R. Environmental, Microbiological, and Immunological Features of Bacterial Biofilms Associated with Implanted Medical Devices. *Clin. Microbiol. Rev.* **2022**, *33* (2), 627−635.

(4) Yuan, L.; Straub, H.; Shishaeva, L.; Ren, Q. Microfluidics for Biofilm Studies. *Annu. Rev. Anal. Chem.* **2023**, *16* (1), 139−159.

(5) Flemming, H.-C.; van Hullebusch, E. D.; Neu, T. R.; Nielsen, P. H.; Seviour, T.; Stoodley, P.; Wingender, J.; Wuertz, S. The Biofilm Matrix: Multitasking in a Shared Space. *Nat. Rev. Microbiol.* **2023**, *21* (2), 70−86.
(6) de Miguel, I.; Prieto, I.; Albornoz, A.; Sanz, V.; Weis, C.; Turon, P.; Quidant, R. Plasmon-Based Biofilm Inhibition on Surgical Implants. *Nano Lett.* **2019**, *19* (4), 2524−2529.
(7) Villegas, M.; Alonso-Cantu, C.; Rahmani, S.; Wilson, D.; Hosseinidoust, Z.; Didar, T. F. Antibiotic-Impregnated Liquid-Infused Coatings Suppress the Formation of Methicillin-Resistant *Staphylococcus aureus Biofilms*. *ACS Appl. Mater. Interfaces* **2021**, *13* (24), 27774−27783.
(8) Skovdal, S. M.; Jørgensen, N. P.; Petersen, E.; Jensen-Fangel, S.; Ogaki, R.; Zeng, G.; Johansen, M. I.; Wang, M.; Rohde, H.; Meyer, R. L. Ultra-Dense Polymer Brush Coating Reduces *Staphylococcus epidermidis* Biofilms on Medical Implants and Improves Antibiotic Treatment Outcome. *Acta Biomater.* **2018**, *76*, 46−55.
(9) Liu, D.; Xi, Y.; Yu, S.; Yang, K.; Zhang, F.; Yang, Y.; Wang, T.; He, S.; Zhu, Y.; Fan, Z.; Du, J. A Polypeptide Coating for Preventing Biofilm on Implants by Inhibiting Antibiotic Resistance Genes. *Biomaterials* **2023**, *293*, 121957−121969.
(10) Geng, H.; Yuan, Y.; Adayi, A.; Zhang, X.; Song, X.; Gong, L.; Zhang, X.; Gao, P. Engineered Chimeric Peptides with Antimicrobial and Titanium-Binding Functions to Inhibit Biofilm Formation on Ti Implants. *Biomater. Adv.* **2018**, *82*, 141−154.
(11) Chu, X.; Yang, F.; Tang, H. Recent Advance in Polymer Coatings Combating Bacterial Adhesion and Biofilm Formation†. *Chin. J. Chem.* **2022**, *40* (24), 2988−3000.
(12) Mao, S.; Zhang, D.; He, X.; Yang, Y.; Protsak, I.; Li, Y.; Wang, J.; Ma, C.; Tan, J.; Yang, J. Mussel-Inspired Polymeric Coatings to Realize Functions from Single and Dual to Multiple Antimicrobial Mechanisms. *ACS Appl. Mater. Interfaces* **2021**, *13* (2), 3089−3097.
(13) Shibata, Y.; Yamashita, Y.; Tsuru, K.; Ishihara, K.; Fukazawa, K.; Ishikawa, K. Preventive Effects of a Phospholipid Polymer Coating on PMMA on Biofilm Formation by Oral Streptococci. *Appl. Surf. Sci.* **2016**, *390*, 602−607.
(14) Mi, G.; Shi, D.; Wang, M.; Webster, T. J. Reducing Bacterial Infections and Biofilm Formation Using Nanoparticles and Nanostructured Antibacterial Surfaces. *Adv. Healthcare Mater.* **2018**, *7* (13), 1800103−1800125.
(15) Butler, J.; Handy, R. D.; Upton, M.; Besinis, A. Review of Antimicrobial Nanocoatings in Medicine and Dentistry: Mechanisms of Action, Biocompatibility Performance, Safety, and Benefits Compared to Antibiotics. *ACS Nano* **2023**, *17* (8), 7064−7092.
(16) Chen, L.; Song, X.; Xing, F.; Wang, Y.; Wang, Y.; He, Z.; Sun, L. A Review on Antimicrobial Coatings for Biomaterial Implants and Medical Devices. *J. Biomed. Nanotechnol.* **2020**, *16* (6), 789−809.
(17) Chen, X.; Ling, X.; Liu, G.; Xiao, J. Antimicrobial Coating: Tracheal Tube Application. *Int. J. Nanomed.* **2022**, *17*, 1483−1494.
(18) Sahoo, J.; Sarkhel, S.; Mukherjee, N.; Jaiswal, A. Nanomaterial-Based Antimicrobial Coating for Biomedical Implants: New Age Solution for Biofilm-Associated Infections. *ACS Omega* **2022**, *7* (50), 45962−45980.
(19) Zhang, L.; Yu, Y.; Zheng, S.; Zhong, L.; Xue, J. Preparation and Properties of Conductive Bacterial Cellulose-Based Graphene Oxide-Silver Nanoparticles Antibacterial Dressing. *Carbohydr. Polym.* **2021**, *257*, 117671−117679.
(20) Zheng, H.; Ji, Z.; Roy, K. R.; Gao, M.; Pan, Y.; Cai, X.; Wang, L.; Li, W.; Chang, C. H.; Kaweeteerawat, C.; Chen, C.; Xia, T.; Zhao, Y.; Li, R. Engineered Graphene Oxide Nanocomposite Capable of Preventing the Evolution of Antimicrobial Eesistance. *ACS Nano* **2019**, *13* (10), 11488−11499.
(21) Zeng, X.; McCarthy, D. T.; Deletic, A.; Zhang, X. Silver/Reduced Graphene Oxide Hydrogel as Novel Bactericidal Filter for Point-of-Use Water Disinfection. *Adv. Funct. Mater.* **2015**, *25* (27), 4344−4351.
(22) Teixeira-Santos, R.; Belo, S.; Vieira, R.; Mergulhõo, F. J. M.; Gomes, L. C. Graphene-Based Composites for Biomedical Applications: Surface Modification for Enhanced Antimicrobial Activity and Biocompatibility. *Biomolecules* **2023**, *13* (11), 1571−1587.
(23) Zhou, Y.; Yang, J.; He, T.; Shi, H.; Cheng, X.; Lu, Y. Highly Stable and Dispersive Silver Nanoparticle−Graphene Composites by a Simple and Low-Energy-Consuming Approach and Their Antimicrobial Activity. *Small* **2013**, *9* (20), 3445−3454.
(24) Pusty, M.; Rana, A. K.; Kumar, Y.; Sathe, V.; Sen, S.; Shirage, P. Synthesis of Partially Reduced Graphene Oxide/Silver Nanocomposite and Its Inhibitive Action on Pathogenic Fungi Grown under Ambient Conditions. *Chemistryselect* **2016**, *1* (14), 4235−4245.
(25) Mukherjee, S.; Bytesnikova, Z.; Martin, S.; Svec, P.; Ridoskova, A.; Pekarkova, J.; Seguin, C.; Weickert, J.; Messaddeq, N.; Mély, Y.; Richtera, L.; Anton, H.; Adam, V. Silver Nanoparticle-Decorated Reduced Graphene Oxide Nanomaterials Exert Membrane Stress and Induce Immune Response to Inhibit the Early Phase of HIV-1 Infection. *Adv. Mater. Interfaces* **2022**, *10* (6), 2201996−2202010.
(26) Crane, M. J.; Devine, S.; Jamieson, A. M. Graphene Oxide/Silver Nanoparticle Ink Formulations Rapidly Inhibit Influenza a Virus and Oc_{43} Coronavirus Infection in Vitro. *bioRxiv* - Microbiology **2021**, 432893 DOI: .
(27) Chen, Y.-N.; Hsueh, Y.-H.; Hsieh, C.-T.; Tzou, D.-Y.; Chang, P.-L. Antiviral Activity of Graphene-Silver Nanocomposites against Non-Enveloped and Enveloped Viruses. *Int. J. Env. Res. Public Health* **2016**, *13* (4), 430−441.
(28) de Faria, A. F.; Martinez, D. S. T.; Meira, S. M. M.; de Moraes, A. C. M.; Brandelli, A.; Filho, A. G. S.; Alves, O. L. Anti-Adhesion and Antibacterial Activity of Silver Nanoparticles Supported on Graphene Oxide Sheets. *Colloid. Surface. B* **2014**, *113*, 115−124.
(29) Zhao, R.; Kong, W.; Sun, M.; Yang, Y.; Liu, W.; Lv, M.; Song, S.; Wang, L.; Song, H.; Hao, R. Highly Stable Graphene-Based Nanocomposite (GO-PEI-Ag) with Broad-Spectrum, Long-Term Antimicrobial Activity and Antibiofilm Effects. *ACS Appl. Mater. Interfaces* **2018**, *10* (21), 17617−17629.
(30) Gupta, A.; Holoidovsky, L.; Thamaraiselvan, C.; Thakur, A. K.; Singh, S. P.; Meijler, M. M.; Arnusch, C. J. Silver-doped Laser-induced Graphene for Potent Surface Antibacterial Activity and Anti-biofilm Action. *Chem. Commun.* **2019**, *55* (48), 6990−6893.
(31) Pipattanachat, S.; Qin, J.; Rokaya, D.; Thanyasrisung, P.; Srimaneepong, V. Biofilm Inhibition and Bactericidal Activity of Niti Alloy Coated with Graphene Oxide/Silver Nanoparticles Via Electrophoretic Deposition. *Sci. Rep.* **2021**, *11* (1), 14008−14016.
(32) Zhang, X.; Mikkelsen, O. Graphene Oxide/Silver Nanocomposites as Antifouling Coating on Sensor Housing Materials. *J. Cluster Sci.* **2022**, *33* (2), 627−635.
(33) Pounraj, S.; Somu, P.; Paul, S. Chitosan and Graphene Oxide Hybrid Nanocomposite Film Doped with Silver Nanoparticles Efficiently Prevents Biofouling. *Appl. Surf. Sci.* **2018**, *452*, 487−497.
(34) Singhal, A. V.; Malwal, D.; Thiyagarajan, S.; Lahiri, I. Antimicrobial and Antibiofilm Activity of GNP-Tannic Acid-Ag Nanocomposite and Their Epoxy-Based Coatings. *Prog. Org. Coat.* **2021**, *159*, 106421−106428.
(35) Kim, A.; Hak Kim, J.; Patel, R. Modification Strategies of Membranes with Enhanced Anti-Biofouling Properties for Wastewater Treatment: A Review. *Bioresour. Technol.* **2022**, *345*, 126501−126512.
(36) Liu, S.; Cao, S.; Guo, J.; Luo, L.; Zhou, Y.; Lin, C.; Shi, J.; Fan, C.; Lv, M.; Wang, L. Graphene Oxide−Silver Nanocomposites Modulate Biofilm Formation and Extracellular Polymeric Substance (EPS) Production†. *Nanoscale* **2018**, *10* (41), 19603−19611.
(37) Le, P. H.; Nguyen, D. H. K.; Aburto-Medina, A.; Linklater, D. P.; Crawford, R. J.; MacLaughlin, S.; Ivanova, E. P. Nanoscale Surface Roughness Influences *Candida albicans* Biofilm Formation. *ACS Appl. Bio. Mater.* **2020**, *3* (12), 8581−8591.
(38) Tang, L.; Pillai, S.; Revsbech, N. P.; Schramm, A.; Bischoff, C.; Meyer, R. L. Biofilm Retention on Surfaces with Variable Roughness and Hydrophobicity. *Biofouling* **2011**, *27* (1), 111−121.
(39) Zhou, K.; Li, Y.; Zhang, L.; Jin, L.; Yuan, F.; Tan, J.; Yuan, G.; Pei, J. Nano-Micrometer Surface Roughness Gradients Reveal Topographical Influences on Differentiating Responses of Vascular

https://doi.org/10.1021/jacsau.4c00008
JACS Au 2024, 4, 855−864

Cells on Biodegradable Magnesium. *Biomater. Adv.* **2021**, *6* (1), 262−272.
(40) Majhy, B.; Priyadarshini, P.; Sen, A. K. Effect of Surface Energy and Roughness on Cell Adhesion and Growth - Facile Surface Modification for Enhanced Cell Culture. *RSC Adv.* **2021**, *11* (25), 15467−15476.
(41) Le, P. H.; Nguyen, D. H. K.; Aburto-Medina, A.; Linklater, D. P.; Crawford, R. J.; MacLaughlin, S.; Ivanova, E. P. Nanoscale Surface Roughness Influences *Candida Albicans* Biofilm Formation. *ACS Applied. Bio Materials.* **2020**, 3 (12), 8581−8591.
(42) Dharmaraja, A. T. Role of Reactive Oxygen Species (ROS) in Therapeutics and Drug Resistance in Cancer and Bacteria. *J. Med. Chem.* **2017**, *60* (8), 3221−3240.
(43) Gao, F.; Shao, T.; Yu, Y.; Xiong, Y.; Yang, L. Surface-Bound Reactive Oxygen Species Generating Nanozymes for Selective Antibacterial Action. *Nat. Commun.* **2021**, *12* (1), 745−762.
(44) Schnaider, L.; Toprakcioglu, Z.; Ezra, A.; Liu, X.; Bychenko, D.; Levin, A.; Gazit, E.; Knowles, T. P. J. Biocompatible Hybrid Organic/Inorganic Microhydrogels Promote Bacterial Adherence and Eradication in Vitro and in Vivo. *Nano Lett.* **2020**, *20* (3), 1590−1597.
(45) Feng, L.; Liu, Y.; Chen, Y.; Xiang, Q.; Huang, Y.; Liu, Z.; Xue, W.; Guo, R. Injectable Antibacterial Hydrogel with Asiaticoside-Loaded Liposomes and Ultrafine Silver Nanosilver Particles Promotes Healing of Burn-Infected Wounds. *Adv. Healthcare Mater.* **2023**, *12* (22), 2203201−2203216.
(46) Wierzbicki, M.; Jaworski, S.; Sawosz, E.; Jung, A.; Gielerak, G.; Jaremek, H.; Łojkowski, W.; Woźniak, B.; Stobiński, L.; Małolepszy, A.; Chwalibog, A. Graphene Oxide in a Composite with Silver Nanoparticles Reduces the Fibroblast and Endothelial Cell Cytotoxicity of an Antibacterial Nanoplatform. *Nanoscale Res. Lett.* **2019**, *14* (1), 320−330.

https://doi.org/10.1021/jacsau.4c00008
JACS Au 2024, 4, 855−864